13th International Symposium on Turbulence and Shear Flow Phenomena (TSFP13)
Montreal, Canada, June 25-28, 2024

NUMERICAL SIMULATION OF BOUNDARY LAYER FLOW ON A FLAT PLATE WITH TURBULENT STIMULATOR

Youhei Takagi
Department of System Design for Ocean-Space
Yokohama National University
79-5 Tokiwadai, Hodogaya-ku, Yokohama,
Kanagawa, 240-8501, Japan
takagi-yohei-hn@ynu.ac.jp

ABSTRACT

To evaluate the availability of traditional turbulence stimulator in the towing tank test by using model ship at very low speed condition, we carried out a direct numerical simulation for boundary layer flow with a trapezoidal stud. The two Reynolds numbers were tested by changing inflow speed, and mean and turbulent properties were investigated at some downstream positions from DNS data. At the case of low Reynolds number, turbulence stimulation was weak and fully-developed turbulent boundary layer could not obtained. However, at the case of relatively-large Reynolds number, some spanwise roll vortex structures were mutually interfered and transited to longitudinal three-dimensional turbulent structured. Therefore, the trapezoidal stud was able to realize turbulent stimulation quickly and effectively at high Reynolds number.

INTRODUCTION

In the towing tank experiment for ship design, scaled model ship is often used. The flow field around ship hull considered to be governed with Reynolds and Froude numbers. The Froude numbers between model- and full-scales ships are matched but the Reynolds number are quite different in these two scales. For example, the Reynolds number at real ship with two or three hundred meters is about 109 and one at model ship with two or three hundred meters is about 106. Therefore, the boundary layer at real ship is fully developed turbulence, on the other hands, one at model ship is laminar-turbulence transition state. The aim of towing tank experiment is to estimate the performance of ship propulsion, and the engineers must obtain turbulent boundary layer at model ship. In ship engineering, small structures such as studs are attached on the bow surface of model ship to generate turbulent boundary layer. These structures are called as turbulence stimulator and the general shape and alignment of them are defined in the guideline of the International Towing Tank Conference, ITTC (ITTC, 2002).

Recently, the zero emission of GHG from commercial ships is highly required. New ships in which oil is not used are proposed and developed but its building and running costs are expensive compared with conventional ships. A different way to achieve the zero emission is the usage of very fat ship at low vehicle speed. This low-speed ship can reduce fuel cost and increase loading capacity at one cruise. However, to develop the new ship, ship engineers must carry out a towing tank experiment at the corresponding low Reynolds number. At the Reynolds number for model ship, we do not know whether the conventional turbulence stimulation can generate fully developed turbulent boundary layer. From this background, some researchers are studying the effect of turbulent stimulators for the boundary layer on a flat plate experimentally and numerically. Lee et al. (Lee, 2022) carried out a velocity measurement with LDV in a cavitating circular water tank for a boundary layer flow with cylindrical studs on a flat plate. For the same experimental conditions, Lee et al. (Lee, 2021) carried out a Large-eddy Simulation (LES) at low Reynolds number. In this work, the effect of sub-grid scale model used in LES has not been discussed in detail. In the present our study, we carry out the Direct Numerical Simulation (DNS) of boundary layer flow on a flat plate with studs and investigate the performance of the conventional turbulence stimulation at the condition of low Reynolds number.

NUMERICAL METHOD

The governing equations are the following incompressible Navier-Stokes and continuity equations:

$$\frac{\partial u_i}{\partial t}+\frac{1}{2}\left[\frac{\partial}{\partial x_j}\left(\varepsilon_{ijk}u_j u_k\right)+u_i\frac{\partial u_i}{\partial x_i}\right]=-\frac{1}{\rho}\frac{\partial p}{\partial x_i}+\nu\frac{\partial u_i^2}{\partial x_j \partial x_j} \quad (1)$$

$$\frac{\partial u_i}{\partial x_i}=0 \quad (2)$$

where u_i is velocity, x_i is coordinate, t is time, ρ is density, p is pressure, ν is kinematic viscosity, and ε_{ijk} is the Eddington epsilon. The nonlinear term of Eq. (1) takes a skew-symmetric form for reducing aliasing error. The governing equations were spatially discretized with the high-order compact difference scheme and temporally integrated with the fractional step method (Kim, 1985). The pressure field defined by the poisson equation was directly solved with the Fast Fourier Transform (FFT) in the wave number space. The grid system was non-uniform orthogonal one and the geometry of turbulence stimulators were considered with the immersed boundary method. All simulations were conducted with the turbulent DNS solver, Xcompact3d (Bartholomew et al., 2020).

NUMERICAL CONDITION

The most of turbulence stimulators used in towing tank are stud, and the geometry of stud defined by the ITTC guideline (ITTC, 2002) is cylindrical stud. On the other hand, trapezoidal stud is widely used in Japan, therefore, we also used its geometry in the present simulation. The dimensions of the trapezoidal stud are shown in Fig. 1(b).

The size of the analytical domain was defined based on the thickness of the stud, D, and the streamwise (x) length is 150D, the spanwise (y) length is 8D, and the vertical (z) height is 15D.

A single stud was attached on a flat plate at the downstream position of 8D from the inlet and the periodic boundary was applied in the spanwise direction for considering actual stud alignment as shown in Fig. 1(a). The boundary condition at the outlet was convective outlet one and that at the upper boundary of y = 15D was atmospheric free boundary. On the surface of the flat plate (y = 0) and stud, no-slip boundary condition was applied.

The flow filed calculated in the present study was the boundary layer on a flat plate, but the setting of the inlet velocity was based on the towing tank test with the KRISO Container Ship (KCS) model (the full-scale length, L_f, is 230 m and the model scale, L_m, is 3.0464 m). Firstly, the full-scale design speed of the KCS model, V_s, were determined as V_s = 11.5 kn (high) and V_s = 4.0 kn (low). Then, Froude numbers were calculated at the full scale and the inflow speeds, U_∞, at the model scale were determined under the same Froude numbers. The conditions for the model length, velocities, and nondimensional numbers (Re_D is the Reynolds number based on U_∞ and D) are summarized in Table 1.

The generated computational grid was non-uniform orthogonal one and clustered at the near wall region to capture the smallest turbulent eddy. The grid numbers were 2049 in the x-direction, 257 in the y-direction, and 256 in the z-direction, and the total grid number in the domain was 134,807,808.

All calculations were temporally integrated until fully developed state that the fluid was swept out on the flow pass more than twice, and mean profiles and turbulent statistics were obtained by ensemble average. To evaluate the grid resolution used in the present simulation, the mean friction velocity was calculated ant the grid width in the x- and z-directions and the minimum grid spacing in the y-direction were calculated in the wall unit (Table 2). For comparison, the grid resolution used in the DNS of turbulent boundary layer with cube-roughened wall (Lee, 2011) is also shown in Table 2. The Reynolds numbers, Re_θ, based on momentum thickness at the downstream region of the present study were comparable with that of the calculation by Lee et al. The present grid resolutions were small compared with Lee et al., and we determined that the present simulation had sufficient grid resolution as DNS of turbulent boundary layer with turbulence stimulation.

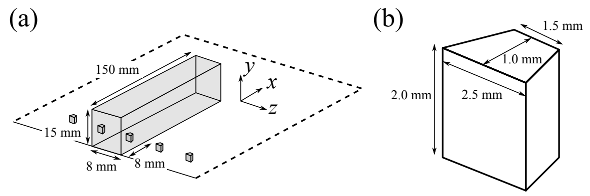

Figure 1. Analysis domain and stud.

Table 1. Numerical condition of the inlet velocity.

L_f [m]	L_m [m]	V_s [kn]	U_∞ [m/s]	Fr	Re_D
230	3.0464	11.5	0.681	0.125	678
230	3.0464	4.0	0.237	0.043	236

Table 2. Grid resolution.

Author	Re_D	Δx^+	Δy^+_{min}	Δz^+
Present	678	1.65	0.137	0.704
Present	236	0.811	0.0672	0.346
Lee et al.	300 (Re_θ)	6.0	0.2	3.0

RESULTS AND DISCUSSION

The mean velocity profiles at the high-speed condition of Re_D = 678 are shown in Figs. 2-3 ant that at the low-speed condition of Re_D = 236 are shown in Figs. 4-5. In these figures, the velocity profiles at x = 45D, 75D, 105D, and 135D are shown because the boundary layer gradually developed at the fluid proceeded in the downward direction. In the present calculations, the spanwise distribution of velocity is not homogenous at laminar-turbulence transient region, and a spanwise spatial average was not taken and ensemble average was done only in time. The theoretical curves for viscous sublayer and logarithmic low region in the turbulent boundary layer are also shown for comparison. The distributions at the middle path between studs (z = 0) are shown in Figs. 2 and 4 and the path just behind a stud (z = 4D) are shown in Figs. 3 and 5. Firstly focusing on the velocity profile at the viscous sublayer, no difference was seen for all points and cases and the grid resolution near the wall was sufficient. In Fig. 2, the logarithmic profiles were obtained except for the position of x = 45D and the turbulence stimulation was sufficient at the middle path at the high Reynolds number of Re_D = 678. On the hand, in Fig. 3, the converge to the logarithmic profile at the downward was weak compared with the results of Fig. 2, and the growth of boundary layer was dependent on the spanwise position even if the inflow speed was high. This weak growth of boundary layer was remarkably seen at the low speed condition shown in Figs. 4-5 and the regions satisfying the logarithmic profile became narrow. Therefore, the turbulence stimulation at the low speed condition for obtaining a turbulent boundary layer was insufficient for the present stud configuration.

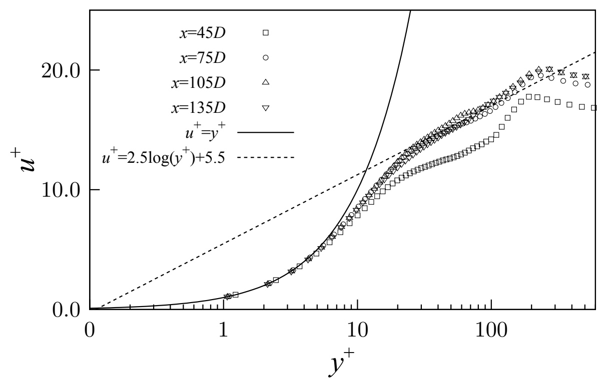

Figure 2. Mean velocity at the middle path between studs for Re_D = 678.

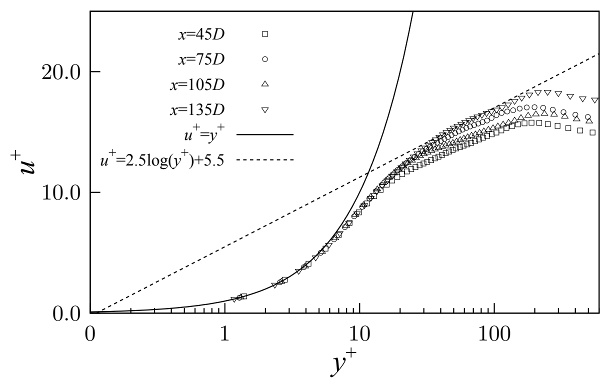

Figure 3. Mean velocity at the path just behind stud for Re_D = 678.

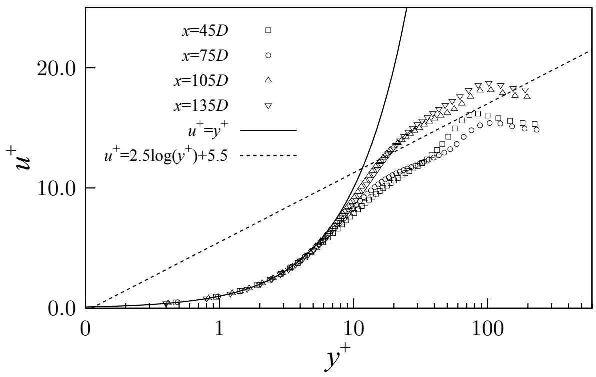

Figure 4. Mean velocity at the middle path between studs for $Re_D = 236$.

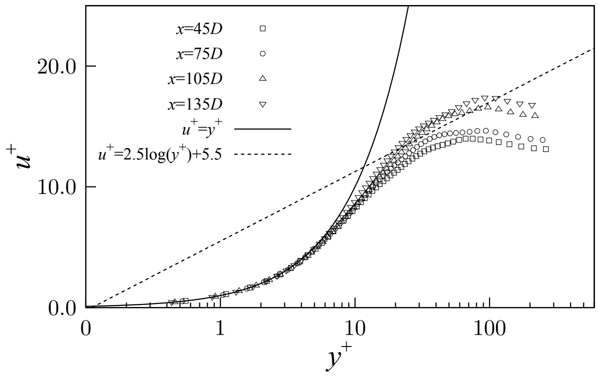

Figure 5. Mean velocity at the path just behind stud for $Re_D = 236$.

To confirm the inhomogenous growth of boundary layer dependent on the local position clearly, the horizontal distribution of the Reynolds number based on momentum thickness is shown in Fig. 6. Although the momentum thickness was suddenly increased at the close region of stud, it was gradually increased in the downward direction for the whole domain. However, the momentum thickness in the middle path of $z = 4D$ was small compared with that in the boundary path of $z = 0$ or $8D$, and it was found that momentum transfer was not homogeneous in the spanwise direction. It seems that the length from the stud to the high homogeneous momentum thickness region takes an important role for efficient turbulence stimulation.

By using the calculated mean velocity at the local horizontal positions, the velocity fluctuations at every time steps were calculated, and the r.ms. values of velocity fluctuations are shown in Figs. 7 and 8. In these figures, the r.ms. values at the three positions of $x = 75D$, $105D$, and $135D$ versus the wall distance normalized with the boundary layer thickness δ, and the other DNS results for the boundary layer with zero-pressure gradient by Wu and Moin (Wu and Moin, 2009) are also shown for comparison. The results only at the high speed condition are shown here but the discussion for the results at the low speed condition for the validity of turbulence stimulation is similar. As shown in Fig. 7(a), the peak values of u^+_{rms} at the middle path take maximum values as same as the high Reynolds number case ($Re_\theta = 300$ and 670) by Wu and Moin and the turbulence stimulation was sufficient for obtaining a strong turbulence intensity for the x-component. As for the y- and z-components, the peak values and locations are well agreed with the corresponding results by Wu and Moin but asymptotic

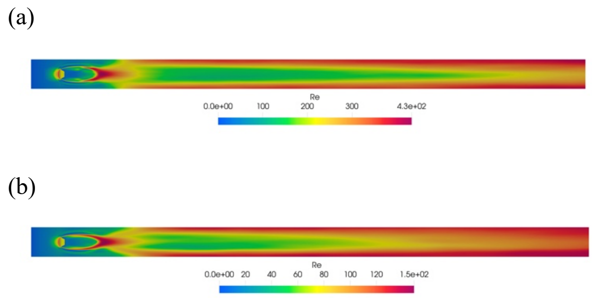

Figure 6. The distribution of Reynolds number based on momentum thickness: (a) $Re_D = 678$ and (b) $Re_D = 236$.

behaviours to zero at the far wall region were not smooth and turbulent intensities took large values at the region more than $y/\delta > 0.5$. On the other hand, at the results at the path just behind stud shown in Fig. 8, the peak values and positions were shifted to the low values and the far y^+ positions from the wall compared with the results of Fig. 7. As same as the discussion for the mean velocity and the momentum thickness, it was found that the generated turbulent intensity was also inhomogeneous in the spanwise direction.

Figure 9 shows a snapshot of the turbulent vortex structure formed behind the stud at the high-speed condition and it is visualized with second invariant of velocity gradient tensor, Q value (Jeong,1995). At the front and root of the stud, a horseshoe-shaped vortex was formed because the inflowed fluid on the flat plane was arrested at the front of the stud and went around the side. At the side edges of the stud, the flow was separated and a large vortex structure including small vortexes was generated. As the flow proceeded into the downward direction, generated small vortexes were aligned with a tilting angle to the wall and coherent hairpin vortexes seen in a fully developed boundary layer were clearly observed shown in Fig. 9(b).

To understand the generation mechanism of turbulent vortical structure due to the stud, the x- and z-components of vorticity are individually visualized in Fig. 10. The region with large value of the streamwise vorticity is corresponded to a three-dimensional longitudinal vortex and the region with large value of the spanwise vorticity to a two-dimensional transverse vortex. As shown in Fig. 10, large transverse vortexes were generated on the root and top of the stud. And then, these two-dimensional vortexes were interfered mutually and the clusters of small longitudinal vortexes was formed at a little apart region from the stud. This scenario of three-dimensional vortexes formation seems to be important for realizing a fast turbulence stimulation with stud.

CONCLUSION

To evaluate the availability of turbulence stimulation with a trapezoidal stud used in towing tank test under a low-speed condition, a direct numerical simulation for the boundary layer flow with the stud was carried out and whether the conventional turbulent stimulation was sufficient or not was investigated. The inflow conditions were set for relatively high speed and low speed conditions corresponding to the tank experiment. At the low speed condition, the logarithmic profile of turbulent boundary layer was not clearly obtained and turbulent stimulation was insufficient. At the high speed condition,

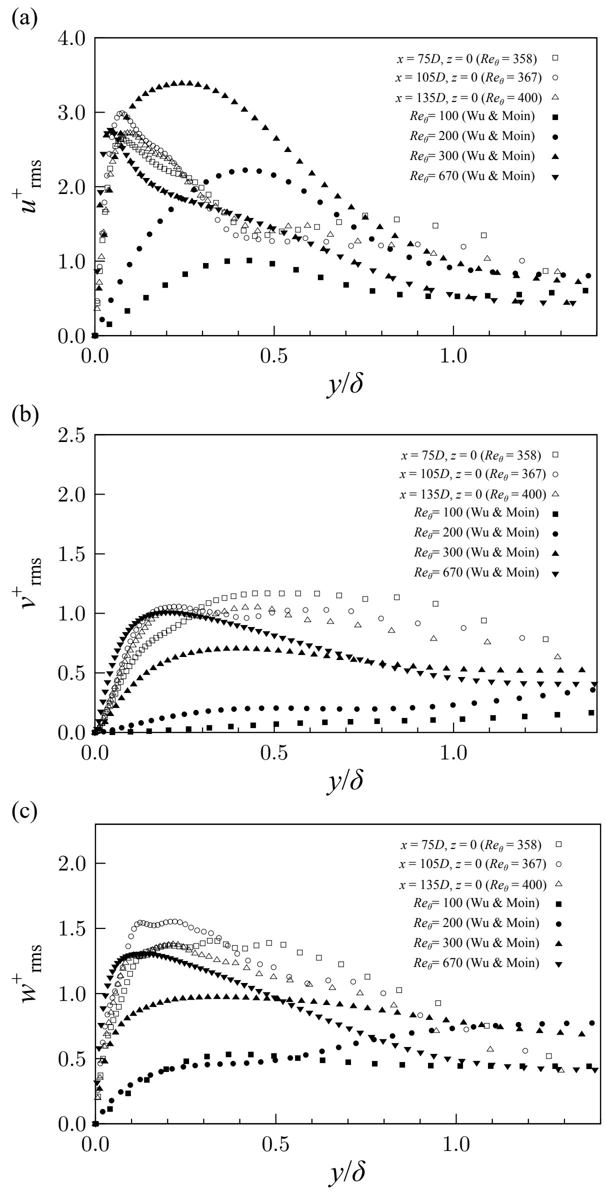

Figure 7. Turbulence intensities at the middle path between studs for Re_D = 678: (a) x-component, (b) y-component, and (c) z-component.

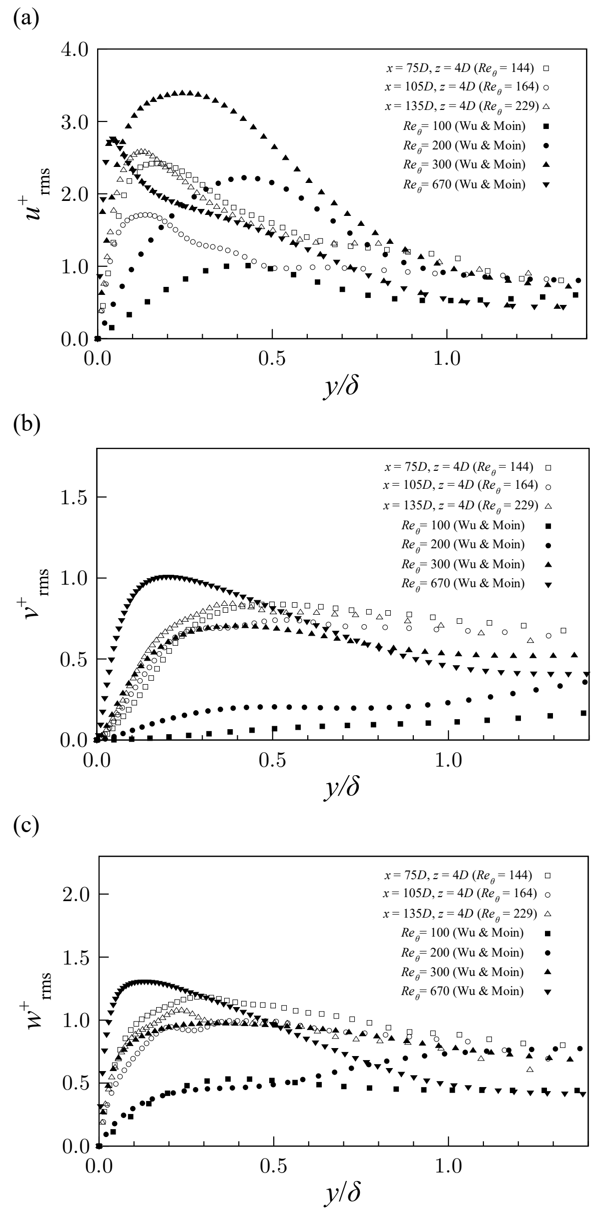

Fig. 8 Turbulence intensities at the path just behind stud for Re_D = 678: (a) x-component, (b) y-component, and (c) z-component.

although flow was transited to turbulence at a downward position, the effect of turbulence stimulation in the spanwise direction was not uniform as same as the low speed condition. The turbulent vortex structures behind the stud was visualized and its formation mechanism was investigated, and it was found that the first generation of two different vortex with spanwise vorticity on the stud took an important role for efficient turbulence stimulation.

ACKNOWLEDGEMENTS

A part of the present study was financially supported by the JSPS KAKENHI (ID:23K26316). As for the large computation, we used the supercomputer, Wisteria/BDEC, by the Information Technology Center, the University of Tokyo.

REFERENCES

Bartholomew, P., Deskos, G., Frantz, R., A., Schuch, F., N., Lamballais, E., and Laizet, S., 2020, "Xcompact3D: An Open-source Framework for Solving Turbulence Problems on a Cartesian Mesh", *SoftwareX*, 12, 100550.

ITTC, 2002, "Recommended Procedures 7.5-01-01-01 Ship Models", 23rd ITTC.

Jeong, J., and Hussain, F., 1995, "On the identification of a vortex", *Journal of fluid mechanics*, 285, 69-94.

Kim, J., and Moin, P., 1985, "Application of a fractional-step method to incompressible Navier-Stokes equations", *Journal of Computational Physics*, 59, 308-323.

Lee, J. H., Sung, H. J., and Krogstad, P. A., 2011, "Direct numerical simulation of the turbulent boundary layer over a cube-roughened wall", *Journal of Fluid Mechanics*, 669, 397-431.

Lee, S. B., Seok, W., and Rhee, S. H., 2021, "Computational Simulations of Transitional Flows around Turbulence Stimulators at Low Speeds", *International Journal of Naval Architecture and Ocean Engineering*, 13, 236-245.

Lee, J. H., Jeong, S. W., and Hwang, S., 2022, "A study on turbulence stimulation effect of studs for boundary layer over a flat plate", *Journal of the Society of Naval Architects of Korea*, 59(1), 18-28.

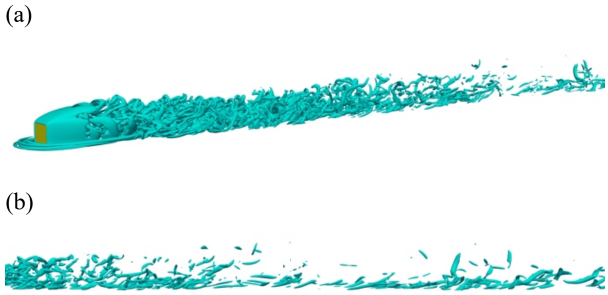

Figure 9 Iso-contours of Q value at Re_D = 678: (a) whole bird view and (b) side view at the latter half region in the downward path.

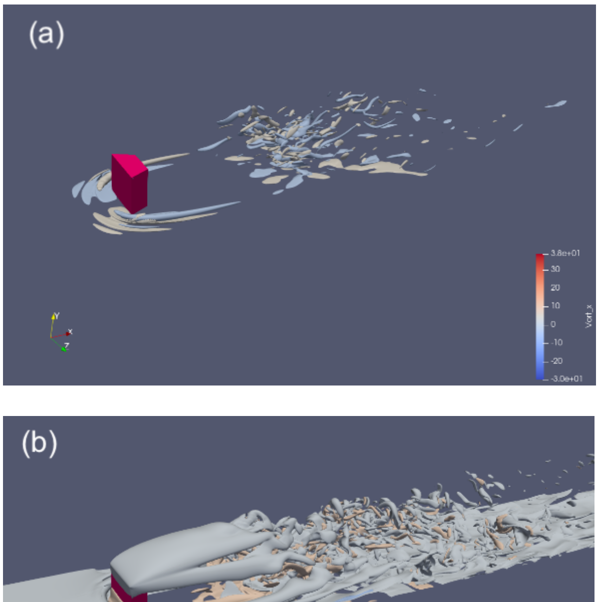

Figure 10. Iso-contours of vorticity at Re_D = 678: (a) streamwise (x) and (b) spanwise (z) components.